

## Research Article

# A Penalized Linear and Nonlinear Combined Conjugate Gradient Method for the Reconstruction of Fluorescence Molecular Tomography

Shang Shang, Jing Bai, Xiaolei Song, Hongkai Wang, and Jaclyn Lau

*Medical Engineering and Health Technology Research Group, Department of Biomedical Engineering, Tsinghua University, Beijing 100084, China*

Received 22 January 2007; Accepted 28 June 2007

Recommended by Jie Tian

Conjugate gradient method is verified to be efficient for nonlinear optimization problems of large-dimension data. In this paper, a penalized linear and nonlinear combined conjugate gradient method for the reconstruction of fluorescence molecular tomography (FMT) is presented. The algorithm combines the linear conjugate gradient method and the nonlinear conjugate gradient method together based on a restart strategy, in order to take advantage of the two kinds of conjugate gradient methods and compensate for the disadvantages. A quadratic penalty method is adopted to gain a nonnegative constraint and reduce the illposedness of the problem. Simulation studies show that the presented algorithm is accurate, stable, and fast. It has a better performance than the conventional conjugate gradient-based reconstruction algorithms. It offers an effective approach to reconstruct fluorochrome information for FMT.

Copyright © 2007 Shang Shang et al. This is an open access article distributed under the Creative Commons Attribution License, which permits unrestricted use, distribution, and reproduction in any medium, provided the original work is properly cited.

## 1. INTRODUCTION

Light with wavelength in the near-infrared range can propagate a few centimeters through the tissue because of low tissue absorption in the spectral of “near-infrared window.” This finding has encouraged the development of fluorescence techniques to visualize specific biochemical events inside living subjects [1, 2]. In recent years, a great development has happened to the fluorescence molecular tomography (FMT), a technique that resolves molecular signatures in deep tissue using fluorescent probes or markers [1, 3–6]. Tissue is illuminated by a series of excitation light in FMT; multiple measurements for the fluorescent emission light are collected from the tissue surface to resolve and quantify fluorochromes deep inside the tissue. With great potential, FMT has become a promising imaging modality for in vivo small animal imaging [1, 2].

Several reconstruction approaches for FMT have been proposed. Most of them are based on the diffusion model [6–10]. The model can be solved by methods such as finite difference method [8], finite element method [6], adaptive finite element method [11], and statistical method [12]. A weighting matrix can be obtained from the forward model, which

describes the influence of each volume element on the detector readings. Generally, the inverse reconstruction problem of FMT is to find the fluorescent source distribution in the target tissue based on the precalculated weighting matrix and the measured data. Since the data measured from the tissue surface is far less than the number of unknown points inside the tissue, the reconstruction problem is illposed, and the solution is sensitive to noise as well as measurement error. Several algorithms have been reported, such as the modified Newton method-based optimization scheme [13] and the Born-type approximation techniques [14]. The conjugate gradient (CG) methods, which need less storage and computation, are favorable for the problems with large-dimension data. They have been reported to be adopted successfully in the reconstruction algorithms for imaging modalities such as the positron emission tomography (PET) [15–17] and diffusion optical tomography (DOT) [18]. Normally, two different kinds of CG with different properties are being used under different conditions. They are the linear CG method (L-CG) and the nonlinear CG method (N-CG) [19]. There is a remarkable point that L-CG and N-CG have reciprocal properties. Combining them together may generate an improved algorithm, which has the advantages of both of them.

In this paper, a penalized linear and nonlinear combined conjugate gradient method (PLN-CG) for the reconstruction of FMT is presented. The L-CG method and the N-CG method are employed separately at different period based on a restart strategy, in order to exert their advantages while compensating for their disadvantages. Besides, a quadratic penalty method is adopted to give the result a nonnegative constraint, as well as reduce the uncertainty and illposedness of the problem. Simulation studies show that the PLN-CG algorithm can give a more accurate and more stable result for the reconstruction in FMT with less computation. Detailed description of the PLN-CG algorithm can be found in Section 3. Section 2 gives a general review of the forward and inverse problems in FMT, including the conventional CG-based reconstruction method. Simulation experiments are presented in Section 4 to demonstrate the validity and efficiency of the proposed algorithm. Section 5 summarizes the main results and gives a general discussion.

## 2. THEORY AND BACKGROUND

### 2.1. Forward model in FMT

When an external excitation light source works at continuous wave mode (CW mode), the following diffusion equation can be employed to model the propagation of the excitation light and the fluorescent emission light [6–10]:

$$\begin{aligned} \nabla \cdot [D_x(\mathbf{r})\nabla\Phi_x(\mathbf{r})] - [\mu_{ax}(\mathbf{r}) + \mu_{af}(\mathbf{r})]\Phi_x(\mathbf{r}) &= -\Theta_s\delta(\mathbf{r} - \mathbf{r}_{sk}), \\ \nabla \cdot [D_m(\mathbf{r})\nabla\Phi_m(\mathbf{r})] - \mu_{am}(\mathbf{r})\Phi_m(\mathbf{r}) &= -\Phi_x(\mathbf{r})\eta\mu_{af}(\mathbf{r}), \end{aligned} \quad (1)$$

where  $\mathbf{r}$  is the position vector belonging to the image region  $\Omega$ .  $\Phi_{x,m}(\mathbf{r})$  represents the photon density at  $\mathbf{r}$  for the excitation light (subscript  $x$ ) or the fluorescent emission light (subscript  $m$ ).  $D_{x,m}(\mathbf{r})$  is defined as the diffusion coefficient

$$D_{x,m}(\mathbf{r}) = (3(\mu_{ax,m}(\mathbf{r}) + (1-g)\mu_{sx,m}(\mathbf{r})))^{-1}, \quad (2)$$

where  $\mu_{ax,m}(\mathbf{r})$  and  $\mu_{sx,m}(\mathbf{r})$  are the absorption and scattering coefficients, respectively.  $g$  is the anisotropy parameter. The absorption of the excitation light due to fluorophores is described as  $\mu_{af}(\mathbf{r})$  and the fluorescent yield  $\eta\mu_{af}(\mathbf{r})$  is required for fluorescence parameter.

### 2.2. The inverse reconstruction problem in FMT

In this work, the finite element method is used to solve the forward model. Detailed description of the finite element method for the FMT forward problem can be found in [6, 11]. Based on the finite element solution of the forward problem, (1) is transformed into a linear matrix equation as follows:

$$\mathbf{W}\mathbf{x} = \mathbf{I}, \quad (3)$$

where  $\mathbf{x}$ , an  $N \times 1$  vector, denotes the real fluorescent source distribution to be reconstructed.  $\mathbf{I}$ , a  $M \times 1$  vector, is the emission data computed from the measurement at the surface of

the tissue. And  $\mathbf{W}$ , a  $M \times N$  matrix, is the weighting matrix generated from the forward model. Generally, the inverse problem for FMT is to find the fluorescent source distribution  $\mathbf{x}$  in the target tissue from the measured data  $\mathbf{I}$  and the precalculated matrix  $\mathbf{W}$ . As mentioned before, the problem in (3) is quite illposed and undetermined.

### 2.3. The L-CG and N-CG method

The implementation of CG in image reconstruction field is generally in two ways. CG is one of the most useful methods for solving large linear systems of equations with symmetric and positive definite parameters, as it is called L-CG [19]. L-CG can be employed in FMT reconstruction by transforming equation (1) into a standard linear system. Since all parameters of each step in L-CG can be obtained from the value of the last step by iterative functions, the computation and storage of the algorithm are reduced. Besides, with pertinence, L-CG converges fast and has a good orientating ability. However, it is brittle and sensitive to noise. The requirement of the standard form of the problem in L-CG limits the implementation of the regularization and penalty methods, which are quite important for the illposed problem in FMT reconstruction. Thus, the CG method for nonlinear optimization problems, namely N-CG, which is more flexible to work along with the regularization and penalty methods and has a better capability to work under noise, is used widely for image reconstruction [15, 17]. According to the least-squares (LS) rule, problem (3) can be changed into a nonlinear optimization problem as follows:

$$\min \phi(\mathbf{x}) = \frac{1}{2} \|\mathbf{I} - \mathbf{W}\mathbf{x}\|^2 + \eta(\mathbf{x}), \quad (4)$$

where  $\eta(\mathbf{x})$  is the regularization or penalty term chosen on various purposes. Then the N-CG method can be adopted to find the optimal solution of (4). However, defects exist in N-CG. This method is more computationally expensive than L-CG, resulting in more time consuming for each iteration. Besides, it converges slowly [20]. Nevertheless, it is noticed that the properties of N-CG and L-CG are reciprocal. Thus, combining N-CG and L-CG together may generate an improved algorithm, which can get a higher speed and accuracy from L-CG as well as a good antinoise capability and the flexibility from N-CG. Therefore, an improved CG-based algorithm for FMT reconstruction, penalized linear and nonlinear combined conjugate gradient method (PLN-CG), was developed according to this consideration. The main scheme of the algorithm is presented in the following section.

## 3. A PENALIZED LINEAR AND NONLINEAR COMBINED CG METHOD

### 3.1. Searching the rough region using L-CG

The searching process for the optimal solution  $\mathbf{x}^*$  in PLN-CG begins with an initial guess  $\mathbf{x}_0$ , and takes a steepest descent first step. The sketch of the scheme is shown in Figure 1.

At first, the search is general and the effect of noise is low, so L-CG is employed to find the rough region of the

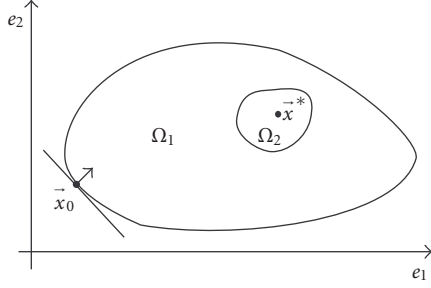


FIGURE 1: The sketch of the combined L-CG and N-CG schemes.

optimal solution  $\mathbf{x}^*$ , that is,  $\Omega_2$ . Because L-CG has a better orientating ability, and needs less computation, it can find  $\Omega_2$  faster and more accurately, while it does not have to expose its fragility under noise.

Transformation has to be made to (3) to make it a standard linear system with symmetric positive definite coefficient matrix. The optimal solution of the LS problem described in (4) satisfies the normal equation as follows:

$$\mathbf{W}^T \mathbf{W} \mathbf{x} = \mathbf{W}^T \mathbf{I}, \quad (5)$$

where  $\mathbf{W}^T$  is the transpose of  $\mathbf{W}$ . Thus

$$\mathbf{W}^* \mathbf{x} = \mathbf{I}^*, \quad (6)$$

where  $\mathbf{W}^* = \mathbf{W}^T \mathbf{W}$ , is an  $N \times N$  symmetric matrix. The reconstruction problem has become a standard linear one, as is required by L-CG.

Starting from an initial guess  $\mathbf{x}_0$ , the solution can be updated iteratively by

$$\mathbf{x}_{k+1} = \mathbf{x}_k + \alpha_k \mathbf{p}_k, \quad (7)$$

where  $\alpha_k$  is the step size

$$\alpha_k = \frac{\mathbf{r}_k^T \mathbf{r}_k}{\mathbf{p}_k^T \mathbf{W}^* \mathbf{p}_k}, \quad (8)$$

and  $\mathbf{r}_k$  is the gradient of each step. It is defined in L-CG as the residue of the linear system, which is obtained iteratively by

$$\mathbf{r}_{k+1} = \mathbf{r}_k + \alpha_k \mathbf{W}^* \mathbf{p}_k, \quad (9)$$

where  $\mathbf{p}_k$  is the searching direction and

$$\begin{aligned} \mathbf{p}_{k+1} &= -\mathbf{r}_{k+1} + \beta_{k+1} \mathbf{p}_k, \\ \beta_{k+1} &= \frac{\mathbf{r}_{k+1}^T \mathbf{r}_{k+1}}{\mathbf{r}_k^T \mathbf{r}_k}. \end{aligned} \quad (10)$$

The L-CG searching iteration process will cease when  $\mathbf{x}_k$  enters the region  $\Omega_2$ . The definition of the region  $\Omega_2$  is determined by a restarting parameter, which is described in the following section.

### 3.2. The restart strategy

The restart strategy is a modification that is often used in nonlinear conjugate gradient procedures [19, 21]. The general scheme is to restart the iteration and take a steepest

descent step according to some predetermined conditions. Restarting serves to periodically refresh the algorithm, erase old information that may not be beneficial or even harmful, and renew the initial guess  $\mathbf{x}_0$  at every restarting time for the new iteration process.

We adopt a restart strategy in the PLN-CG scheme described as follows:

$$|\mathbf{r}_k| = |\mathbf{r}_{k-1} + \alpha_{k-1} \mathbf{W}^* \mathbf{p}_{k-1}| \leq \delta, \quad (11)$$

where  $\mathbf{r}_k$  represents the gradient of  $\phi(\mathbf{x}_k)$ . When  $|\mathbf{r}_k|$  satisfies (11), it means that the  $\mathbf{x}_k$  obtained at current iteration has entered the small region  $\Omega_2$  around  $\mathbf{x}^*$ . Then, a steepest descent step is taken, using the gradient direction at current point as the searching direction. At the same time, a new iteration process with the N-CG method begins, using  $\mathbf{x}_k$  as the initial guess  $\mathbf{x}_0$ . The experiential typical value for  $\delta$  is between  $10^{-3}$  and  $10^{-5}$ . Normally, we choose  $10^{-4}$  for practical use.

### 3.3. Use of the N-CG method

After entering  $\Omega_2$ , the searching result is getting quite closer to the optimal solution, so the effect of noise has to be taken into consideration. Besides, the uncertainty of the searching has increased. Thus, the method has been shifted to N-CG, which can work better with noisy data. Besides, N-CG can introduce the penalty or regularization method to gain a constraint as well as to reduce the illposedness.

Now, problem (3) is transformed into a nonlinear optimization problem:

$$\min \phi(\mathbf{x}) = \frac{1}{2} \|\mathbf{I} - \mathbf{W} \mathbf{x}\|^2 + \eta(\mathbf{x}), \quad (12)$$

where  $\eta(\mathbf{x})$  is a penalty term which will be discussed in Section 3.4.

The N-CG method differs from L-CG mainly in two ways. Firstly, rather than using a standard iterative function to find the step length  $\alpha_k$ , a line search method is used to identify an approximate minimum of the nonlinear function  $\phi(\mathbf{x})$  along the searching direction  $\mathbf{p}_k$  [15, 17, 19]. Secondly, the gradient of  $\phi(\mathbf{x})$  in L-CG is simply the residue of the linear system that can be obtained iteratively. While for N-CG, it must be replaced by the gradient of the nonlinear objective  $\phi(\mathbf{x})$ , that is,  $\nabla \phi(\mathbf{x})$ .

Thus, using the  $\mathbf{x}_k$  obtained from L-CG as the initial guess  $\mathbf{x}_0$  for N-CG, the solution is updated iteratively:

$$\mathbf{x}_{k+1} = \mathbf{x}_k + \alpha_k \mathbf{p}_k, \quad (13)$$

where  $\alpha_k$  is the step size that is computed by a line search method,

$$\min f(\mathbf{x}_k + \alpha \mathbf{p}_k) \quad \text{s.t. } \alpha \geq 0, \quad (14)$$

where  $\mathbf{p}_k$  is the searching direction and

$$\begin{aligned} \mathbf{p}_{k+1} &= -\mathbf{r}_{k+1} + \beta_{k+1} \mathbf{p}_k, \\ \beta_{k+1} &= \frac{\mathbf{r}_{k+1}^T (\mathbf{r}_{k+1} - \mathbf{r}_k)}{\mathbf{r}_k^T \mathbf{r}_k}, \end{aligned} \quad (15)$$

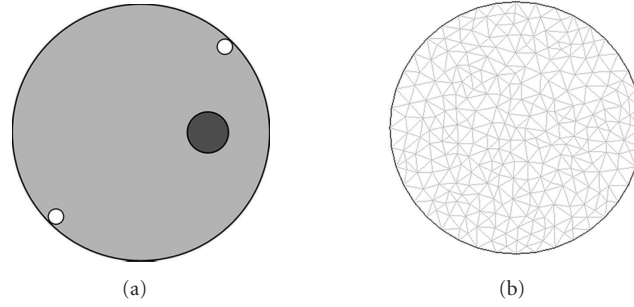


FIGURE 2: (a) Configuration of the simulation experiment using two excitation sources. The object is homogeneous, with a fluorophore (designated with •) imbedded in it. Two excitation sources (designated with ◦) are placed around the inner surface of the object. (b) Mesh in the forward FEM model.

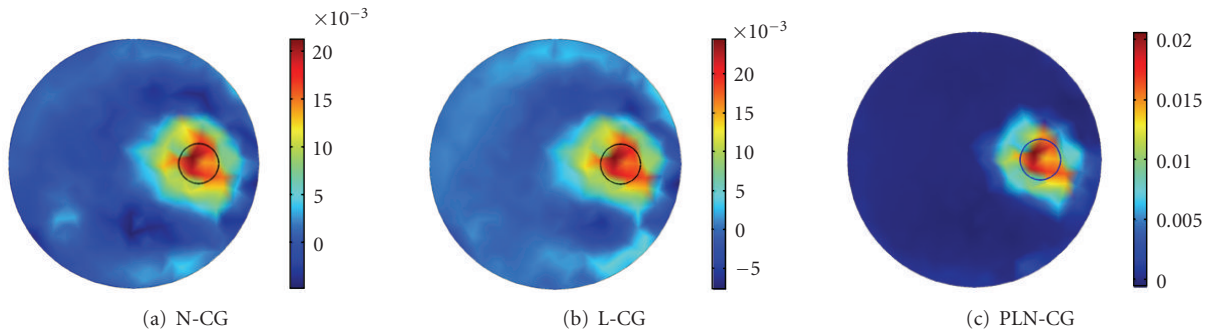


FIGURE 3: Images reconstructed with different methods. (a) N-CG, (b) L-CG, (c) PLN-CG. All results were obtained with a hundred iterations,  $\gamma$  was chosen to be 50. A zero vector was used as the initial guess. The small circle in each figure shows the real distribution of the fluorophore.

where  $\mathbf{r}_k$  is the gradient of the objective function  $\phi(\mathbf{x})$  at current point, that is,

$$\mathbf{r}_k = \nabla \phi(\mathbf{x}_k). \quad (16)$$

### 3.4. The nonnegative penalty

It is known that a major problem of the conventional gradient-based methods is that they are mainly designed for unconstrained problems, but the fluorescent source distribution in the biological tissue has to be constrained to a nonnegative region [16, 22]. Here, a quadratic penalty method [15, 19] is adopted to give the problem a nonnegative constraint.

Consider the penalty function described below

$$\eta = \gamma \sum_i x_i^2 u(-x_i), \quad (17)$$

where  $x_i$  is the  $i$ th element of  $\mathbf{x}$ ,  $u(x)$  is the unit step function. During the searching procedure, when the searched result  $\mathbf{x}$  at current iteration has negative values, the penalty term will be increased. In this way, it will penalize  $\mathbf{x}$  and force it to go back.  $\gamma$  is a penalty weighting parameter, which will gradually become zero as the iteration number increases. Thus, the solution of the new unconstrained problem in (12) with the penalty term (17) will approach the solution of the original problem in (3). The value of  $\gamma$  will be discussed experimentally in Section 4.1.3.

Set an initial value  $\mathbf{x}_0$ , and the restarting parameter  $\delta$ .

- (1) Find  $\mathbf{x}_k$  using L-CG method, the gradient  $\mathbf{r}_k = \mathbf{A}\mathbf{x}_k - \mathbf{b}$ , as in (9).
- (2) If  $\|\mathbf{r}_k\| \leq \delta$ , go to (3). Else, repeat (1).
- (3) Restart, set  $\mathbf{x}_0 = \mathbf{x}_k$ ,  $\beta = 0$ .
- (4) Find the optimal solution  $\mathbf{x}^*$  with N-CG method, use  $\phi(\mathbf{x})$  with penalty function  $\eta(\mathbf{x})$  as the objective function.

ALGORITHM 1: The PLN-CG scheme for FMT reconstruction.

Thus, a penalized linear and nonlinear combined conjugate gradient method is generated according to the scheme described above. The main flow of Algorithm 1 is listed below.

## 4. SIMULATIONS AND RESULTS

### 4.1. Simulations with two sources

In this experiment, a numerical model was set up to test the validity of the PLN-CG algorithm. A circular object was simulated with an outer diameter of 25 mm, which had a fluorophore with a diameter of 4 mm embedded in it. We supposed the optical property to be homogeneous, with  $\mu_a = 0.005 \text{ mm}^{-1}$  and  $\mu_s = 1 \text{ mm}^{-1}$ . In order to show the ef-

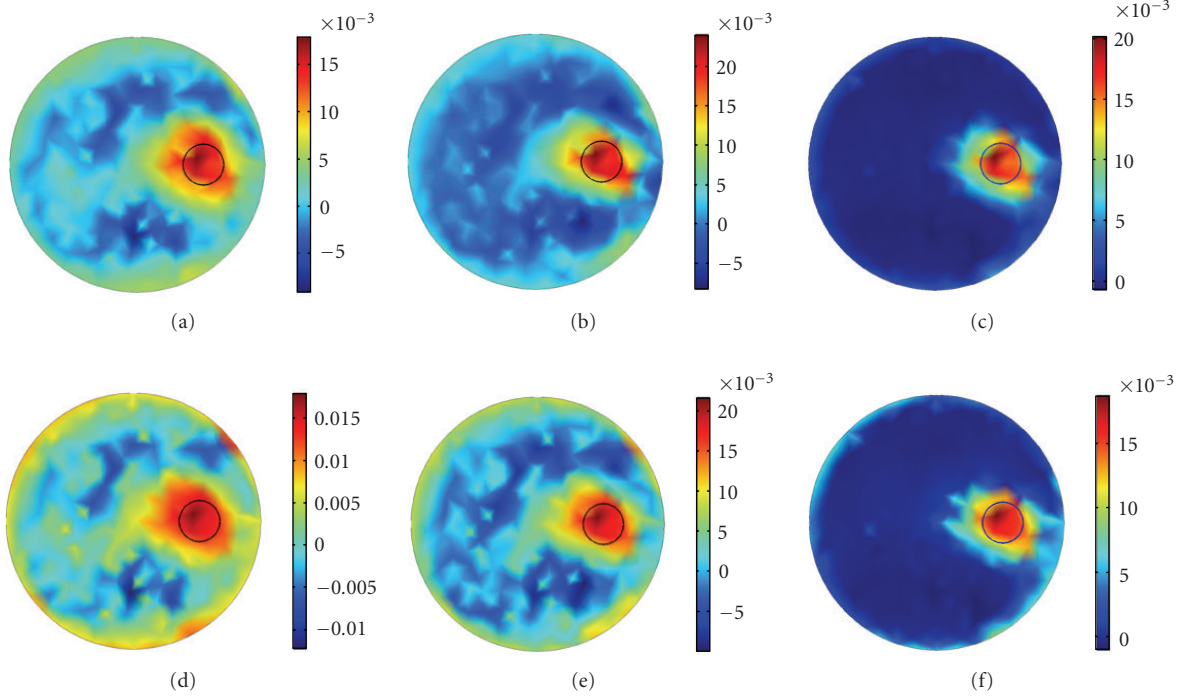


FIGURE 4: Images reconstructed with different initial guesses, using N-CG (Column 1), L-CG (Column 2), and PLN-CG (Column 3). Initial guess for (a)–(c) was an all-0.005 vector, and for (d)–(f) was an all-0.01 vector. Results were all obtained with one hundred iterations.  $\gamma$  was 50 for the PLN-CG approach. The small circle in each figure shows the real distribution of the fluorophore.

efficiency of PLN-CG better, only two excitation sources were used this time. They were placed around the inner surface of the circular object (as shown in Figure 2(a)), and were turned on in turn. For each source, 32 detector readings were available through the detector fibers, which were distributed uniformly on the surface of the circular object.

The forward data were simulated by finite element method [6, 10], using a FEM light transport model in CW mode [7]. The object was divided into 518 small triangular elements and the mesh is shown in Figure 2(b). The FEM forward engine was based on COMSOL Multiphysics (Section 3.2). The reconstruction algorithm was programmed in MATLAB 6.5. A computer with CPU AMD Athlon $\times$ 23600+ and 512M DDRII memory was used.

Images reconstructed by N-CG, L-CG, and PLN-CG are shown in Figures 3(a), 3(b), and 3(c). All images were obtained with one hundred iterations, as the objective function would descend very slowly thereafter. The nonnegative penalty parameter  $\gamma$  used for PLN-CG was 50. A zero vector was used as the initial guess for each algorithm.

It can be seen that images reconstructed by N-CG and L-CG are noisy. Negative values exist, which affect the accuracy of the results. While for PLN-CG, the values are all nonnegative, and the image is cleaner and more accurate. The computing time was about 5.02 seconds for N-CG, 0.22 second for L-CG, and 1.45 seconds for PLN-CG. It indicates that L-CG is much faster than N-CG. So helping N-CG with L-CG has tremendously reduced the computing time, as in the PLN-CG method.

#### 4.1.1. Reconstruction using different initial guesses

Being sensitive to the initial guess is a big disadvantage for most of the iterative approach based algorithms. It is regarded as a standard to test the stability of the algorithm.

Figure 4 shows the results reconstructed with different initial values, using N-CG (Column 1), L-CG (Column 2), and PLN-CG (Column 3), respectively. Since most elements of the original solution are zero and the quantity of the fluorochrome intensity in FMT is relatively small, a zero vector is closer to the solution of the problem and is a better choice to be the initial value (Figure 3). When the initial value is increased to 0.005 and 0.01, the reconstructed images of N-CG (Figures 4(a) and 4(d)) and L-CG (Figures 4(b) and 4(e)) become perturbed, with artifacts distributed in the background. Whereas the PLN-CG (Figures 4(c) and 4(f)) is still giving a clear result, with only a slight blur on the edge.

#### 4.1.2. Reconstruction using noisy data

To test the stability of the algorithm, white Gaussian noise was added to the detector readings. Figure 5 shows the images reconstructed by N-CG (Column 1), L-CG (Column 2), and PLN-CG (Column 3). The L-CG method reveals its fragility under noise. The image is perturbed when the noise level is 5% (Figure 5(e)). When the noise level is 10%, the image is totally blurred, as is shown in Figure 5(h). The N-CG method has a better performance compared with L-CG (Figures 5(i) and 5(g)). However, many artifacts exist in the images and affect the quantification of the fluorophore.

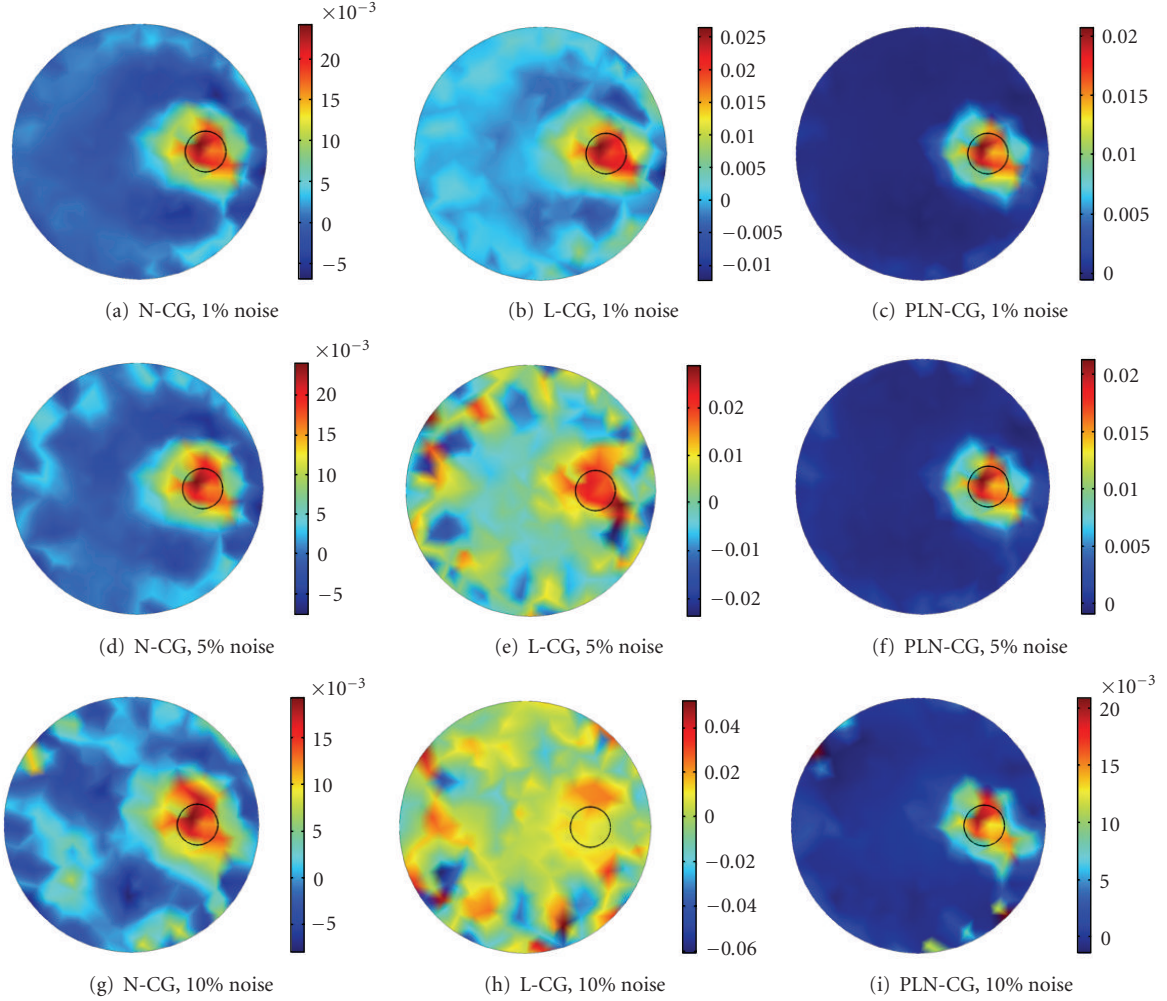


FIGURE 5: Images reconstructed with noisy data, using N-CG (Column 1), L-CG (Column 2), and PLN-CG (Column 3). Noise level for (a)–(c) was 1%, for (d)–(f) was 5%, and for (g)–(i) was 10%. Results reconstructed with N-CG and L-CG were obtained with one hundred and fifty iterations. For PLN-CG, when  $\gamma$  was 50, the iteration number was one hundred. The small circle in each figure shows the real distribution of the fluorophore.

Whereas, images reconstructed with PLN-CG approach are clear when the noise levels are 1% (Figure 5(c)) and 5% (Figure 5(f)). When the noise level is 10%, the fluorescent source distribution is still relatively clear, with a little artifacts appearing on the edge.

#### 4.1.3. The value of the penalty parameter $\gamma$

When using the PLN-CG method,  $\gamma$  is the weighting parameter that controls the effect of the penalty term. Figure 6 shows the images reconstructed with different  $\gamma$ .

It can be seen that when  $\gamma$  is  $10^{-3}$ , the effect of the penalty term is not enough. Negative values exist and the background is not clean. Increasing  $\gamma$  to 1 does produce better results (Figure 6(b)), and a further increase to  $10^3$  enhances the improvement (Figure 6(c)). When  $\gamma$  increases to  $10^5$ , the quality of the image begins to get worse (Figure 6(d)). The results show that the penalty term can work well for a large varia-

tion of  $\gamma$ . A typical value for  $\gamma$  is  $10$  to  $10^3$ . Besides,  $\gamma$  should be increased when the total iteration number increases.

In addition, rather than keeping  $\gamma$  fixed, one can use different  $\gamma$  according to the experiential equation [18]

$$\gamma = an^2, \quad (18)$$

where  $n$  is the iteration number.  $a$  is a fixed weighting parameter, which can be set to a value between  $10^{-3}$  and 1. Figure 6(f) shows the images reconstructed according to (18). The iteration number was one hundred and  $a$  was chosen to be 0.005.

#### 4.2. Simulations with more sources

Simulation studies above were based on two excitation sources, in order to demonstrate the qualities of the PLN-CG approach better. When the number of sources is increased, a larger dataset can be obtained. It will improve the information content of the measurements and reduce

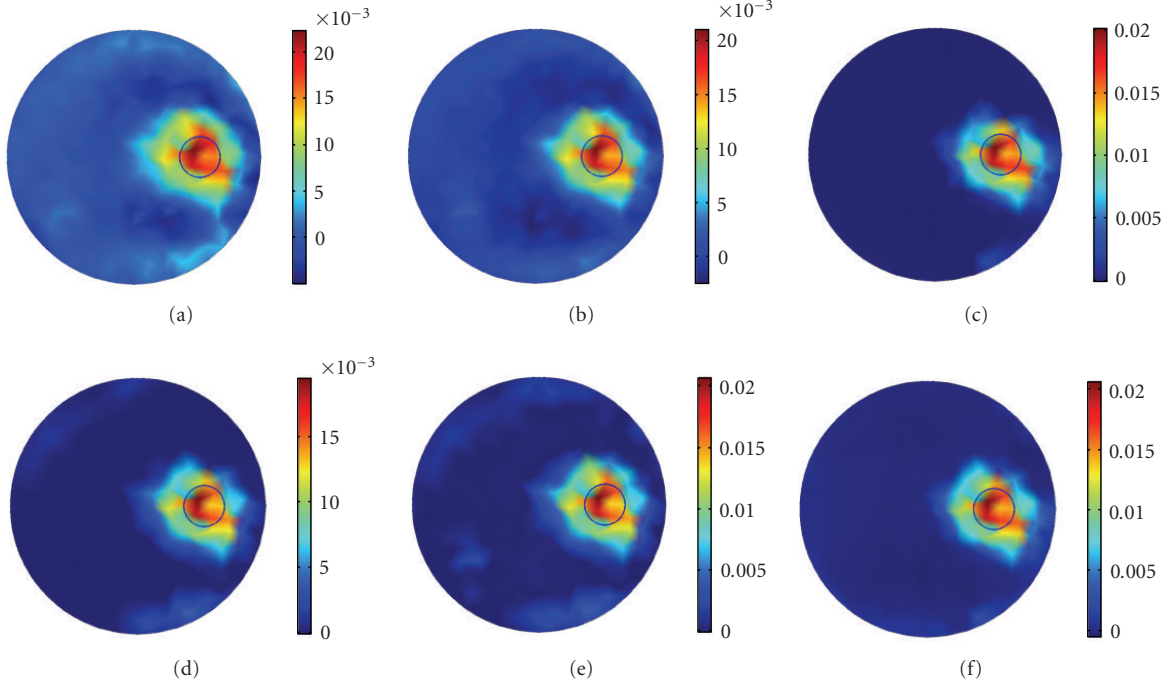


FIGURE 6: Reconstructed images using different  $\gamma$ : (a)  $\gamma = 1e - 3$ ; (b)  $\gamma = 1$ ; (c)  $\gamma = 1e3$ ; (d)  $\gamma = 1e5$ ; (e)  $\gamma = 1e7$ ; (f)  $\gamma = 0.005n^2$ , where  $n$  is the iteration number. A zero vector was used as the initial guess for each reconstruction process, and all results were obtained with a hundred iterations. The small circle in each figure shows the real distribution of the fluorophore.

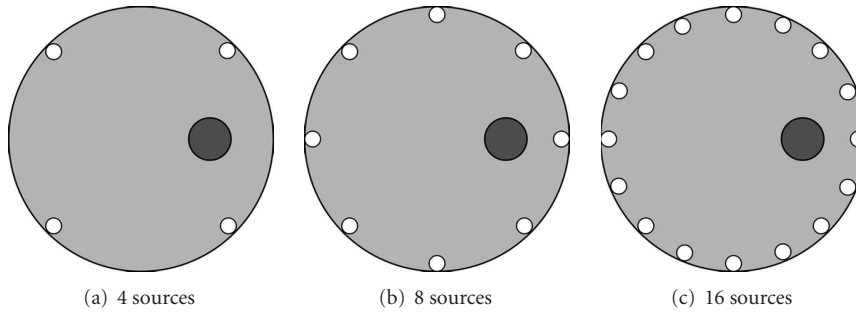


FIGURE 7: Configuration of the simulation experiments using more excitation sources. (a) 4 sources. (b) 8 sources. (c) 16 sources. The excitation sources are distributed uniformly around the inner surface of the object (designated with  $\circ$ ). For each experiment, the object is homogeneous, with a fluorophore (designated with  $\bullet$ ) embedded in it.

the illposedness of the inverse problem [5]. Thus, in practice, FMT equipments normally use more excitation sources [3, 4]. Here, simulation experiments were designed using 4 sources (Figure 7(a)), 8 sources (Figure 7(b)), and 16 sources (Figure 7(c)), respectively.

In each experiment, sources were turned on in turn and 32 detector readings were available for each source. Results with clean data were obtained with a hundred iterations for about 2.99 seconds in the 4 sources case (Figure 8(a)). While the computing time was about 4.9220 seconds and 9.1560 seconds for 150 iterations in the 8 sources case (Figure 8(b)) and 16 sources case (Figure 8(c)), as they have a larger dataset.  $\gamma$  was simply set to 50 for all cases because the difference among the iteration numbers was small. It is shown that as the source number increases, the qualities of the re-

constructed images are in progress. The reconstructed fluorochrome region marked with the small black circle is more even and closer to the original value.

After the experiments using clean data described above, white Gaussian noise with a constant variance was added to the detector readings. The noise level was 10%. It is shown that the reconstructed results become clearer and better when the sources number increases from 2 (Figure 5(i)) to 4 (Figure 8(d)) and 8 (Figure 8(e)). However, when using 16 sources (Figure 8(f)), the image is not improved compared with the 8 sources case, or even worse, which defies the common sense. The reason may be that, when using clean and accurate data for the reconstruction, more datasets mean more information, whereas for the cases using noisy data, too many data may interfere with each other and counteract

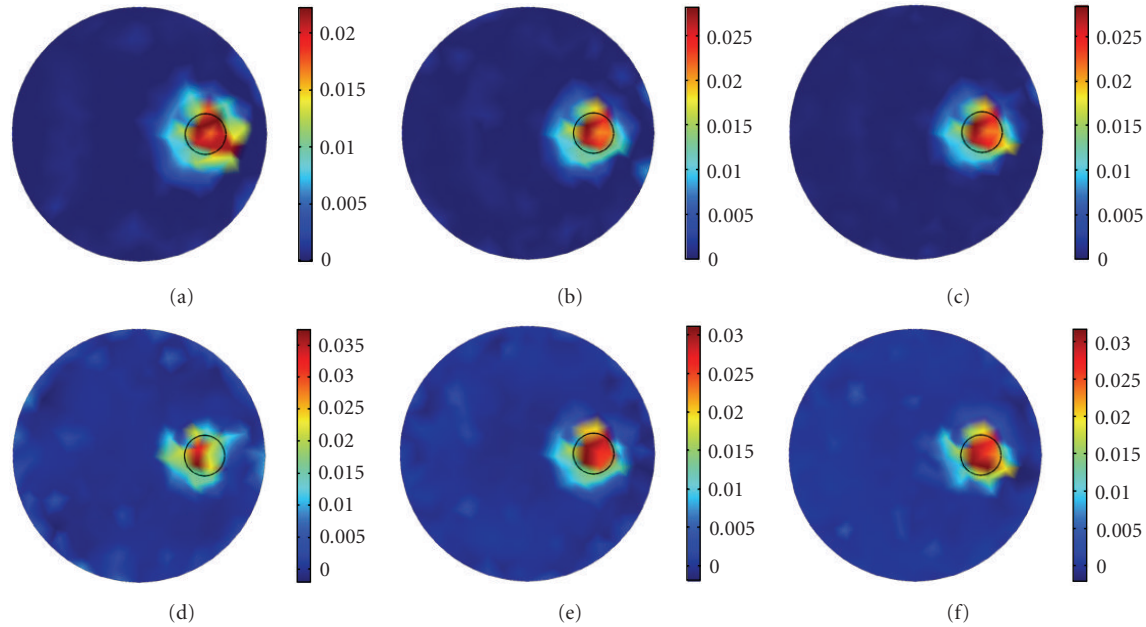


FIGURE 8: Images reconstructed in the experiments which have more excitation sources. (a) 4 sources, clean data; (b) 8 sources, clean data; (c) 16 sources, clean data; (d) 4 sources, 10% noise; (e) 8 sources, 10% noise; (f) 16 sources, 10% noise. The small circle in each figure shows the real distribution of the fluorophore.

the effect. Nevertheless, the results of this experiment further demonstrate the capability of the PLN-CG method to work under noise.

## 5. DISCUSSION AND CONCLUSION

The goal of this work was to establish a fast and accurate algorithm for FMT reconstruction, which is illposed. In order to achieve this goal, a penalized linear and nonlinear combined conjugate gradient algorithm was developed. Simulation studies have indicated that this PLN-CG method can exhibit very favorable performance and produce relatively stable behavior. Further studies show that, when using sixteen sources, the reconstruction algorithm can work under 15% noise, which is sufficient for practical use. The better performance is partly achieved by the combination of L-CG and N-CG. L-CG makes the algorithm faster and more accurate. While at the same time, N-CG gives the whole algorithm a better capacity to deal with noise. It introduces the penalty method to get a nonnegative constraint and reduce the uncertainty of the problem. The restart strategy also improves the efficiency of the algorithm by refreshing the algorithm periodically.

Further improvement can be made for the PLN-CG algorithm in future. Some kind of regularization techniques can be employed to regularize the results and smoothen the images [6]. The prior knowledge about the intensity of the fluorochrome can be used to utilize a general threshold of the reconstructed fluorescent source density to decrease the permissible region [11]. In addition, doing more restarting procedures appropriately may also upgrade the reconstruction images. Currently, we are involved in the practical use of

the PLN-CG reconstruction algorithm for the ongoing FMT experiment in our laboratory.

## ACKNOWLEDGMENTS

This work is partially supported by the National Nature Science Foundation of China, the Tsinghua-Yue-Yuen Medical Science Foundation, the National Basic Research Program of China, and the Special Research Fund for the Doctoral Program of Higher Education of China.

## REFERENCES

- [1] V. Ntziachristos, C. Bremer, and R. Weissleder, "Fluorescence imaging with near-infrared light: new technological advances that enable in vivo molecular imaging," *European Radiology*, vol. 13, no. 1, pp. 195–208, 2003.
- [2] V. Ntziachristos, J. Ripoll, L. V. Wang, and R. Weissleder, "Looking and listening to light: the evolution of whole-body photonic imaging," *Nature Biotechnology*, vol. 23, no. 3, pp. 313–320, 2005.
- [3] V. Ntziachristos and R. Weissleder, "Charge-coupled-device based scanner for tomography of fluorescent near-infrared probes in turbid media," *Medical Physics*, vol. 29, no. 5, pp. 803–809, 2002.
- [4] V. Ntziachristos, C.-H. Tung, C. Bremer, and R. Weissleder, "Fluorescence molecular tomography resolves protease activity in vivo," *Nature Medicine*, vol. 8, no. 7, pp. 757–760, 2002.
- [5] E. E. Graves, J. Ripoll, R. Weissleder, and V. Ntziachristos, "A submillimeter resolution fluorescence molecular imaging system for small animal imaging," *Medical Physics*, vol. 30, no. 5, pp. 901–911, 2003.
- [6] A. X. Cong and G. Wang, "A finite-element-based reconstruction



- tion method for 3D fluorescence tomography,” *Optics Express*, vol. 13, no. 24, pp. 9847–9857, 2005.
- [7] S. R. Arridge, M. Schweiger, M. Hiraoka, and D. T. Delpy, “A finite element approach for modeling photon transport in tissue,” *Medical Physics*, vol. 20, no. 2, pp. 299–309, 1993.
- [8] D. Y. Paithankar, A. U. Chen, B. W. Pogue, M. S. Patterson, and E. M. Sevick-Muraca, “Imaging of fluorescent yield and lifetime from multiply scattered light reemitted from random media,” *Applied Optics*, vol. 36, no. 10, pp. 2260–2272, 1997.
- [9] X. Song, J. Yi, and J. Bai, “A parallel reconstruction scheme in fluorescence tomography based on contrast of independent inversed absorption properties,” *International Journal of Biomedical Imaging*, vol. 2006, Article ID 70839, 7 pages, 2006.
- [10] X. Song, X. Xiong, and Z. Zhang, “A fast pre-iteration reconstruction method for 3D fluorescence tomography based on finite element analysis,” in *The 5th Annual Meeting of the Society for Molecular Imaging*, The Big Island of Hawaii, Hawaii, USA, August–September 2006.
- [11] A. Joshi, W. Bangerth, K. Hwang, J. C. Rasmussen, and E. M. Sevick-Muraca, “Fully adaptive FEM based fluorescence optical tomography from time-dependent measurements with area illumination and detection,” *Medical Physics*, vol. 33, no. 5, pp. 1299–1310, 2006.
- [12] A. B. Milstein, S. Oh, K. J. Webb, et al., “Fluorescence optical diffusion tomography,” *Applied Optics*, vol. 42, no. 16, pp. 3081–3094, 2003.
- [13] W. Cong, D. Kumar, Y. Liu, A. Cong, and G. Wang, “A practical method to determine the light source distribution in bioluminescent imaging,” in *Developments in X-Ray Tomography IV*, vol. 5535 of *Proceedings of SPIE*, pp. 679–686, Denver, Colo, USA, October 2004.
- [14] V. Ntziachristos and R. Weissleder, “Experimental three-dimensional fluorescence reconstruction of diffuse media by use of a normalized born approximation,” *Optics Letters*, vol. 26, no. 12, pp. 893–895, 2001.
- [15] E. U. Mumcuoglu, R. Leahy, S. R. Cherry, and Z. Zhou, “Fast gradient-based methods for Bayesian reconstruction of transmission and emission PET images,” *IEEE Transactions on Medical Imaging*, vol. 13, no. 4, pp. 687–701, 1994.
- [16] E. U. Mumcuoglu and R. Leahy, “A gradient projection conjugate gradient algorithm for Bayesian PET reconstruction,” in *IEEE Nuclear Science Symposium and Medical Imaging Conference*, vol. 3, pp. 1212–1216, Norfolk, Va, USA, October–November 1994.
- [17] J. A. Fessler and S. D. Booth, “Conjugate-gradient preconditioning methods for shift-variant PET image reconstruction,” *IEEE Transactions on Image Processing*, vol. 8, no. 5, pp. 688–699, 1999.
- [18] A. H. Hielscher, A. D. Klose, and K. M. Hanson, “Gradient-based iterative image reconstruction scheme for time-resolved optical tomography,” *IEEE Transactions on Medical Imaging*, vol. 18, no. 3, pp. 262–271, 1999.
- [19] J. Nocedal and S. J. Wright, *Numerical Optimization*, Springer, New York, NY, USA, 2000.
- [20] A. J. Davies, D. B. Christianson, L. C. W. Dixon, R. Roy, and P. van der Zee, “Reverse differentiation and the inverse diffusion problem,” *Advances in Engineering Software*, vol. 28, no. 4, pp. 217–221, 1997.
- [21] M. J. D. Powell, “Restart procedures for the conjugate gradient method,” *Mathematical Programming*, vol. 12, no. 1, pp. 241–254, 1977.
- [22] M. Hanke, J. G. Nagy, and C. Vogel, “Quasi-Newton approach to nonnegative image restorations,” *Linear Algebra and Its Applications*, vol. 316, no. 1–3, pp. 223–236, 2000.

## Special Issue on Video Analysis for Human Behavior Understanding

### Call for Papers

Video cameras are becoming increasingly ubiquitous and pervasive in our daily life. Along with the fast growing number of exchanged and archived videos, there is an urgent need for advanced video analysis techniques that can systematically interpret and understand the semantics of video contents, within the application domains of security surveillance, intelligent transportation, health/home care, video indexing/retrieving, video summarization/highlighting, and so on. Understanding human behaviors based on video analysis calls for even greater challenges due to very large variations of human bodies and their motion activities under all kinds of contexts such as different viewing perspectives, dressing colors, changing human poses, human-human occlusions, and body parts self-occlusions. To overcome these challenges, not only the traditional image processing, computer vision, pattern recognition, and machine learning techniques are required, but also advanced estimation theory and statistical inference, articulated 2D/3D human body modeling and synthesis, sophisticated database or rules for events/behaviors, and so on are critically desired.

The primary focus of this special issue will be on the advanced video analysis techniques for understanding human behaviors, starting from human object detection, segmentation and tracking, 2D/3D spatial and temporal features extraction, 2D/3D human body modeling and synthesis, event discovery and behavior learning, system performance evaluation, and potential applications of these techniques. The special issue is intended to become an international forum for researches to summarize the most recent developments and ideas in the field. The topics to be covered include, but are not limited to:

- Modern wireless communication system techniques such as multiantenna and multiaccess, spectrum sensing and cognitive radio, wireless ad hoc and sensor networks, cooperative signal processing, and information theory
- Human object detection and segmentation
- Tracking of human objects
- Tracking under multiple cameras
- Crowd estimation and crowd behavior analysis
- Occlusions and segmentation errors handling

- 2D/3D articulated human body modeling
- Modeling and learning of human behaviors
- Knowledge interpretations of human behaviors

Before submission authors should carefully read over the journal's Author Guidelines, which are located at <http://www.hindawi.com/journals/asp/guidelines.html>. Prospective authors should submit an electronic copy of their complete manuscript through the journal Manuscript Tracking System at <http://mts.hindawi.com/> according to the following timetable:

Manuscript Due	December 15, 2009
First Round of Reviews	March 15, 2010
Publication Date	June 15, 2010

### Lead Guest Editor

**Jenq-Neng Hwang**, Department of Electrical Engineering, Box 352500, University of Washington, Seattle, WA 98195, USA; [hwang@u.washington.edu](mailto:hwang@u.washington.edu)

### Guest Editors

**Changick Kim**, Department of Electrical Engineering, Korea Advanced Institute of Science and Technology (KAIST), Daejeon 305-701, South Korea; [cikim@ee.kaist.ac.kr](mailto:cikim@ee.kaist.ac.kr)

**Hsu-Yung Cheng**, Department of Computer Science and Information Engineering, National Central University, Jhongli, Taiwan; [chengsy@csie.ncu.edu.tw](mailto:chengsy@csie.ncu.edu.tw)

## Special Issue on Advances in Random Matrix Theory for Signal Processing Applications

### Call for Papers

In recent years, the mathematical field of random matrix theory (RMT) has emerged as an extremely powerful tool for a variety of signal processing applications. Recent advances, both in the areas of exact (finite-dimensional) and asymptotic (large-dimensional) RMTs, have received strong interest from amongst the signal processing community and have been instrumental for a number of recent breakthroughs. For example, advances in RMT techniques have paved the way for the design of powerful multiantenna and multiuser signal processing modules which are currently revolutionizing the field of wireless communications; they have led to fundamental insights into the information-theoretic limits (achievable by any signal processing strategy) in multidimensional wireless channels; they have pushed forward the development of advanced synthetic aperture radar (SAR) imaging techniques; they have provided the key ingredient for designing powerful new detection and estimation techniques in array signal processing.

This Special Issue aims to bring together state-of-the-art research contributions that address open problems in signal processing using RMT methods. While papers that are primarily of mathematical interest will be considered, the main focus is on applications of these techniques to real-world signal processing problems. Potential topics include (but are not limited to) the following areas:

- Modern wireless communication systems techniques, such as multiantenna and multiaccess, spectrum sensing and cognitive radio, wireless ad hoc and sensor networks, cooperative signal processing, information theory
- Detection and estimation, array processing
- Radar, MIMO radar, SAR imaging, and remote sensing

Before submission authors should carefully read over the journal's Author Guidelines, which are located at <http://www.hindawi.com/journals/asp/guidelines.html>. Prospective authors should submit an electronic copy of their complete manuscript through the journal Manuscript Tracking Sys-

tem at <http://mts.hindawi.com/>, according to the following timetable:

Manuscript Due	November 1, 2009
First Round of Reviews	February 1, 2010
Publication Date	May 1, 2010

### Lead Guest Editor

**Matthew McKay**, Department of Electronic and Computer Engineering, Hong Kong University of Science and Technology, Clear Water Bay, Hong Kong; [eemckay@ust.hk](mailto:eemckay@ust.hk)

### Guest Editors

**Marco Chiani**, Department of Electronics, Computer Sciences and Systems, University of Bologna, 40136 Bologna, Italy; [mchiani@deis.unibo.it](mailto:mchiani@deis.unibo.it)

**Raj Rao Nadakuditi**, Department of Electrical Engineering and Computer Science, University of Michigan, 1301 Beal Avenue, Ann Arbor, MI 48109-2122, USA; [rajrao.umich@gmail.com](mailto:rajrao.umich@gmail.com)

**Christ Richmond**, Lincoln Laboratory, Massachusetts Institute of Technology, Lexington, MA 02420-9108, USA; [christ@ll.mit.edu](mailto:christ@ll.mit.edu)

**Peter Smith**, Department of Electrical and Computer Engineering, University of Canterbury, Christchurch 8140, New Zealand; [peter.smith@canterbury.ac.nz](mailto:peter.smith@canterbury.ac.nz)

## Special Issue on Multicamera Information Processing: Acquisition, Collaboration, Interpretation, and Production

### Call for Papers

Video sensors have gained in resolution, quality, cost-efficiency, and ease of use during the last decade, thus fostering the deployment of rich acquisition settings, to cheaply and effectively capture scenes at high spatiotemporal resolution, in multiple locations and directions. By providing extended and redundant coverage, multicamera imaging provides a practical approach to support robust scene interpretation, integrated situation awareness, as well as rich interactive and immersive experience in many different areas of industry, health-care, education, and entertainment. Tools and algorithms that aim to recognize high-level semantic concepts and their spatiotemporal and causal relations directly depend on the robustness and reliability of the underlying detection and tracking methods. These tasks related to scene interpretation have a strong impact on many real-life applications and are also fundamental to understand how to render a scene, for example, in a sport event summarization context or while browsing multiview video surveillance content. Finally, multiview imaging allows for immersive visualization by adapting rendered images to display capabilities and/or viewer requests. The goal of this special issue is to present the recent theoretical and practical advances that take advantage of multiview processing to improve 3D scene monitoring, immersive rendering, and (semi-)automatic content creation. Topics of interest include, but are not limited to:

- Acquisition of multiview and 3D images
- Multicamera information fusion
- Automated extraction of calibration or geometry information
- Distributed scene representation and communication
- Depth estimates and arbitrary view synthesis
- Multiview object detection and tracking
- Multiview video stream events/activities mining
- Multiview event detection and recognition
- Assistance to interactive video browsing in a distributed surveillance camera network
- Immersive rendering, and 3D scene virtual navigation

- Automatic and/or personalized summarization of sports events
- Plants or impaired people monitoring applications
- Advanced application case studies

Before submission authors should carefully read over the journal's Author Guidelines, which are located at <http://www.hindawi.com/journals/ivp/guidelines.html>. Prospective authors should submit an electronic copy of their complete manuscript through the journal Manuscript Tracking System at <http://mts.hindawi.com/> according to the following timetable:

Manuscript Due	December 1, 2009
First Round of Reviews	March 1, 2010
Publication Date	June 1, 2010

#### Lead Guest Editor

**Christophe De Vleeschouwer**, UCL, Louvain-la-Neuve, Belgium; [christophe.devleeschouwer@uclouvain.be](mailto:christophe.devleeschouwer@uclouvain.be)

#### Guest Editors

**Andrea Cavallaro**, Queen Mary, University of London, London, UK; [andrea.cavallaro@elec.qmul.ac.uk](mailto:andrea.cavallaro@elec.qmul.ac.uk)

**Pascal Frossard**, EPFL, Lausanne, Switzerland; [pascal.frossard@epfl.ch](mailto:pascal.frossard@epfl.ch)

**Li-Qun Xu**, British Telecommunications PLC, London, UK; [li-qun.xu@bt.com](mailto:li-qun.xu@bt.com)

**Peter Tu**, GE Global Research, Niskayuna, NY, USA; [tu@crd.ge.com](mailto:tu@crd.ge.com)